Polymer translocation in an environment of active rods

Hamidreza Khalilian [1,*], Jalal Sarabadani [1,†] and Tapio Ala-Nissila [2,3]

[1]*School of Nano Science, Institute for Research in Fundamental Sciences (IPM), 19395-5531 Tehran, Iran*
[2]*Department of Applied Physics and QTF Center of Excellence, Aalto University, P.O. Box 11000, FI-00076 Aalto, Espoo, Finland*
[3]*Interdisciplinary Centre for Mathematical Modelling and Department of Mathematical Sciences,
Loughborough University, Loughborough, Leicestershire LE11 3TU, United Kingdom*

We consider the dynamics of a translocation process of a flexible linear polymer through a nanopore into an environment of active rods in the *trans* side. Using Langevin dynamics simulations, we show that the rods facilitate translocation to the *trans* side even when there are initially more monomers on the *cis* than on the *trans* side. Structural analysis of the translocating polymer reveals that active rods induce a folded structure to the *trans*-side subchain in the case of successful translocation events. By keeping the initial number of monomers on the *cis*-side subchain fixed, we map out a state diagram for successful events as a function of the rod number density for a variety of system parameters. This reveals competition between facilitation by the rods at low densities and crowding that hinders translocation at higher densities.

I. INTRODUCTION

Polymer translocation through a synthetic or biological nanopore has become an active field of research since the seminal experimental works by Bezrukov *et al.* in 1994 [1] and two years later by Kasianowicz *et al.* [2], and the theoretical study by Sung and Park [3] in 1996. It has attracted a lot of interest from both experimental [4–12] and theoretical points of view [13–46]. The translocation process has many applications in different areas, such as transport of mRNA through nuclear membrane pores [47], drug delivery and DNA sequencing [48–50], and gene transfer between bacteria [51]. Biological polymers often translocate through a nanopore embedded in a membrane into an environment composed of other biological organisms [52], such as diffusive or fixed spherical obstacles [53–56], chaperons [57–59], and other biomolecules or even micro-organisms.

The nature of the dynamics of polymer translocation depends on the details of the setup. There are multiple different scenarios, including the *pore-driven* case [21,22,26,28], wherein the external driving force only acts on those monomers inside the nanopore, the *end-pulled* case [25,30], in which the external driving force acts on the head monomer of the polymer either by atomic force microscope [60] or by optical or magnetic tweezers [5,9,61,62], and the *unbiased* case, with no external drive [33–35]. In biological

*khalilian@ipm.ir
†jalal@ipm.ir

systems chaperons and other active agents can strongly influence translocation processes. To this end, pore-driven polymer translocation into an environment of active spherical particles has been studied, and it has been shown numerically that the crowding effect in two dimensions increases the translocation speed provided that the activity of the particles is high enough [63]. Also, using the same model, the translocation time has been obtained as a function of the size of spherical active particles, and the most favorable case occurs when the size of the active particles is comparable to the segment (monomer) size of the polymer [64]. In addition, in Ref. [45] the rectification of unbiased translocation of a polymer due to the presence of chiral active particles was studied.

In the externally unbiased translocation process there must be an effective driving force on the chain to overcome the repulsive entropic force. Without an external drive, an imbalance may come from a net attractive entropic force due to unequal fluctuations of the spatial configurations of the polymer between the *cis* and the *trans* sides [33–35]. For example, the presence of chaperons [57], attractive binding particles [44], or active particles [65] in the *trans* side may lead to a directed motion of the polymer either to the *cis* or to the *trans* side, depending on the values of the system parameters [44,63,65]. In particular, we have recently shown in Ref. [65] that active rodlike particles in the *trans* side can induce an effective driving force which facilitates translocation when part of the chain is initially in the *trans* side. Using extensive computer simulations and the iso-flux tension propagation (IFTP) theory, we obtained the scaling form of the mean translocation time as a function of the initial polymer contour length in the *cis* side, the rod activity, and the rod length [65].

In Ref. [65] the initial contour length of the chain in the *trans* side was fixed to a constant value of $N_{02} = 100$ monomers while the other relevant parameters were varied such that translocation events were successful. An interesting
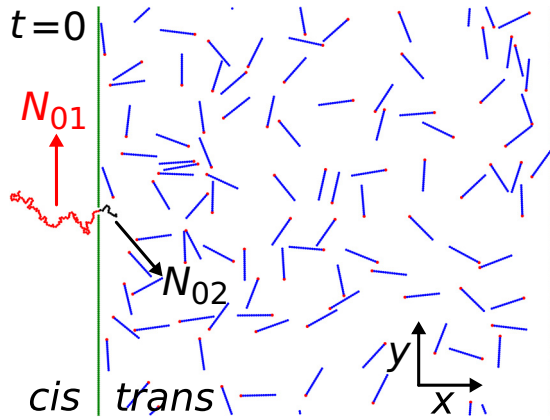
FIG. 1. Configuration of the system after equilibration and before the actual translocation process. N_{01} and N_{02} are the initial contour lengths of the *cis*- and *trans*-side polymer subchains, respectively. After equilibration the self-propelling (SP) force F_{sp} is switched on and acts on the head of each rod (filled red circles in the *trans* side) from its tail to its head. In all simulations, the initial *cis*-side subchain contour length is fixed at $N_{01} = 100$. There is one monomer at the pore and thus the total contour length of the polymer is $N_0 = N_{01} + N_{02} + 1$. The directions perpendicular and parallel to the membrane (green vertical line) are denoted by x and y, respectively.

question then remains concerning the role of N_{02} in determining successful translocation events. To this end, in the present work we use extensive Langevin dynamics simulations to investigate this issue. While the initial contour length of the *cis*-side subchain is fixed at $N_{01} = 100$, the contour length of the polymer subchain in the *trans* side N_{02} is varied together with other system parameters. This allows us to map out a "state diagram" with a boundary separating successful and failed translocation events.

A particularly interesting finding in our work is that due to their shape anisotropy the rods may align with the membrane and induce folds on the *trans*-side polymer subchain. This facilitates directed translocation towards the *trans* side for cases where $N_{02} < N_{01}$, which would not be possible without the active rods. The state diagram also reveals that for fixed N_{01}, the boundary between successful and unsuccessful events has nonmonotonic dependence on the number density of the rods due to rod crowding, which will eventually hinder translocation for higher densities.

The paper is structured as follows. The Langevin dynamics (LD) simulation model is explained in detail in Sec. II. Section III is devoted to the numerical results. Finally, our Summary and Conclusions can be found in Sec. IV.

II. SIMULATION MODEL

We consider a two-dimensional simulation box of size $L_x = 400\sigma$ and $L_y = L_x/2$ in the x and y directions, respectively (see Fig. 1). A one-dimensional membrane composed of particles with size σ separated by σ from each other divides the simulation box in the y direction. A nanopore of radius 1.5σ is located at $x = y = 0$ in the membrane. A flexible linear polymer with a total number of monomers N_0 modeled by the bead-spring model [66] is set in the simulation box

such that one of its monomers is inside the nanopore. The *cis*- and *trans*-side subchains contain N_{01} and N_{02} monomers, respectively, and $N_0 = N_{01} + N_{02} + 1$. In the *trans* side, there are N_r rigid rods, each composed of L_r beads with diameter σ. Two walls (constructed similar to the membrane) parallel to the y direction are located at $x = -200\sigma$ and $x = 200\sigma$, and periodic boundary conditions are applied in the y direction.

The bonded interaction between consecutive monomers in the polymer is a combination of a finitely extensible nonlinear elastic (FENE) potential,

$$U_{FENE}(r) = -\frac{1}{2}kR_0^2 \ln\left(1 - r^2/R_0^2\right), \tag{1}$$

where k, R_0, and r are the spring constant, the maximum allowed distance, and the distance between the consecutive monomers, respectively, and the Weeks-Chandler-Anderson (WCA) potential

$$U_{WCA}(r) = \begin{cases} U_{LJ}(r) - U_{LJ}(r_c), & r < r_c; \\ 0, & r \geqslant r_c, \end{cases} \tag{2}$$

where $r_c = 2^{1/6}\sigma$ is the cut-off radius. The term $U_{LJ}(r)$ is the Lennard-Jones (LJ) potential

$$U_{LJ}(r) = 4\varepsilon\left[\left(\frac{\sigma}{r}\right)^{12} - \left(\frac{\sigma}{r}\right)^6\right], \tag{3}$$

with ε and r as the potential well depth and the distance between two given particles, respectively. The nonbonded monomers as well as the monomers and the wall particles, and also membrane particles and the rod beads, interact each other via the WCA excluded volume interaction.

The LD equation is employed to describe the dynamics of the position of the ith monomer of the polymer as

$$M\ddot{\vec{r}}_i = -\eta\dot{\vec{r}}_i - \vec{\nabla}U_{mi} + \vec{\xi}_i(t), \tag{4}$$

where η and U_{mi} are the solvent friction coefficient and the sum of all interactions for the ith monomer, respectively. $\vec{\xi}_i$ is the white noise with $\langle\vec{\xi}_i(t)\rangle = \vec{0}$ and $\langle\vec{\xi}_i(t) \cdot \vec{\xi}_j(t')\rangle = 4\eta k_B T \delta_{ij}\delta(t - t')$, where k_B, T, δ_{ij}, and $\delta(t - t')$ are the Boltzmann constant, the temperature, and the Kronecker and Dirac delta functions, respectively.

The time evolution of the ith bead of each rod is governed by the following Langevin equation:

$$M\ddot{\vec{r}}_i = -\eta\dot{\vec{r}}_i + F_{SP}\delta_{ih}\hat{e} - \vec{\nabla}U_{ri} + \vec{\xi}_i(t), \tag{5}$$

where F_{SP} and h stand for the self-propelling (SP) force and the head bead of the rod, respectively, $\hat{e}$ is the unit vector parallel to the rod's main axis from the tail to the head bead, and U_{ri} is the sum of all interactions on the ith bead of the rod.

M, σ, and ε are employed as the units for mass, length, and energy, respectively. In our simulations, we use $M = 1$ as mass of each monomer in the polymer and bead in the rod, and set $\sigma = 1$ and $\varepsilon = 1$. The temperature is kept at $k_B T = 1.2$, and the solvent friction coefficient is $\eta = 0.7$. The integration time step is $dt = 0.001\tau_0$, where $\tau_0 = \sqrt{M\sigma^2/\varepsilon}$ is the simulation time unit. The spring constant is set to $k = 30$, and $R_0 = 1.5$. The LAMMPS package [67] was used to perform the simulations, and the results were averaged over 2000 uncorrelated trajectories.
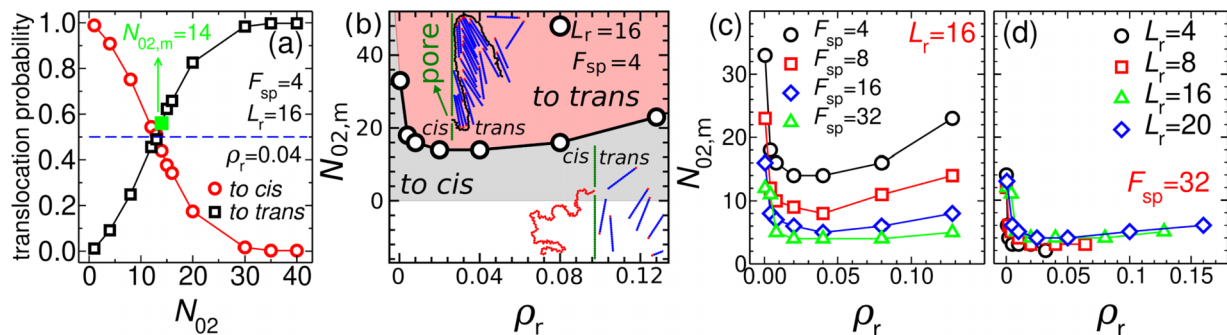
FIG. 2. (a) The probability of polymer translocation through a nanopore back to the *cis* side (open red circles) and into the *trans* side (open black squares) as a function of the initial value of the polymer subchain contour length in the *trans* side, N_{02}, for fixed values of $L_r = 16$, $F_{sp} = 4$, and $\rho_r = 0.04$ ($N_r = 100$). The filled green square at $N_{02,m} = 14$ represents the boundary between the *to-cis* and *to-trans* states. The horizontal blue dashed-line is plotted at $1/2$. (b) A diagram showing the regions of *to-cis* and *to-trans* states in the $N_{02,m} - \rho_r$ plane for fixed values of $L_r = 16$ and $F_{sp} = 4$. The open black circles connected by the solid line denote the boundary between the two regions. The top and the bottom insets show snapshots of final configurations of the system in the vicinity of the nanopore for a fixed value of $N_{02,m} = 14$. (c) Additional diagrams in the $N_{02,m} - \rho_r$ plane separating the *to-trans* (above the curves) from the *to-cis* (below the curves) events for $L_r = 16$ and various values of $F_{sp} = 4$ (black line - circles), 8 (red line - squares), 16 (blue line - diamonds), and 32 (green line - triangles). (d) The same as in panel (c) but for fixed $F_{sp} = 32$ and different values of $L_r = 4$ (black line - circles), 8 (red line - squares), 16 (green line - triangles), and 20 (blue line - diamonds).

In our model each bead size corresponds to the single-stranded DNA Kuhn length, which is about 1.5 nm, and the interaction strength at room temperature $T = 295$ K is 3.39×10^{-21} J. Thus, the timescales and force in LJ units are approximately 32.1 ps and 2.3 pN, respectively.

Before starting the actual translocation process, when the monomer inside the pore is fixed such that there are N_{01} and N_{02} monomers in the *cis* and *trans* sides of the simulation box, respectively, and in the absence of the SP force, the system is equilibrated for $t_{eq} = 5 \times 10^4 \tau_0$ (see Appendix A). Then, after equilibration, the polymer is released and the SP force F_{sp} is simultaneously switched on for all the rods. The number density of the active rods (ARs) is given by $\rho_r = L_r N_r/(L_x L_y/2)$, and it is low enough such that after equilibration the rods are in a spatially uniform isotropic phase.

For all simulations, the initial length of the polymer subchain in the *cis* side is fixed at $N_{01} = 100$, and at fixed values of F_{sp} and ρ_r the value of N_{02} (initial length of the polymer subchain in the *trans* side) has been varied to find its minimum value for which more than 50% of the translocation events to the *trans* side are successful. The LD simulations were performed for the SP force $F_{sp} = 32$ with the rod lengths $L_r = 4, 8, 16$, and 20, and also for the rod length $L_r = 16$ with SP forces $F_{sp} = 4, 8, 16$, and 32, including $N_r = 1, 10, 20, 50, 100, 200$, and 320 ARs in the *trans* side of the simulation box.

III. RESULTS

Figure 1 shows a typical snapshot of the system just before the translocation process at $t = 0$ in the equilibrium state with the rods in the isotropic phase. When the SP force is switched on, the combination of alignment of the ARs with the membrane as well as interaction between ARs and the *trans*-side polymer subchain induces a net effective force towards the *trans* side [65] (see Appendix B). Therefore a tension front propagates along the backbone of the *cis*-side subchain while

the polymer is sucked by the environment of ARs into the *trans* side. This mechanism allows the polymer to overcome the entropic barrier and facilitates the translocation process, provided that the initial contour length of the polymer subchain in the *trans* side is long enough (e.g., $N_{02} = 100$ in our previous work [65]).

In the present work we focus on the influence of the initial contour length of the *trans*-side polymer subchain on the dynamics of the translocation process. To this end, we keep the initial contour length of the *cis*-side polymer subchain constant at $N_{01} = 100$. When 50% or more of the translocation attempts are successful, we label the corresponding parameter sets as *to-trans* states while the unsuccessful events are labeled as *to-cis* states.

A. Dependence of translocation events on system parameters

In order to distinguish between the *to-trans* and *to-cis* states, the values of the parameters such as N_r, L_r, and F_{sp} are kept fixed and the length of polymer subchain in the *trans* side N_{02} is varied. By finding the minimum value of N_{02} that is labeled $N_{02,m}$ at which the translocation is *to-trans*, we can draw a diagram on the $N_{02,m} - \rho_r$ plane for fixed values of L_r and F_{sp}.

Figure 2(a) shows the probability of polymer translocation into or out of the active environment in the *trans* side as a function of the initial value of the *trans*-side polymer subchain contour length N_{02} for fixed values of $L_r = 16$, $F_{sp} = 4$, and $\rho_r = 0.04$ corresponding to $N_r = 100$. By increasing the value of N_{02}, the probability of translocation into the *trans* side increases (black squares) while the probability of failed events decreases (red circles). The filled green square denoted by $N_{02,m} = 14$ identifies the boundary wherein for $N_{02} < N_{02,m}$ the translocation event is *to-cis* state, and for $N_{02} \geqslant N_{02,m}$ the state is *to-trans*.

Panel (b) in Fig. 2 shows the state diagram in the $N_{02,m} - \rho_r$ plane for fixed values of $L_r = 16$ and $F_{sp} = 4$. The value of N_r has been varied and the diagram obtained from the
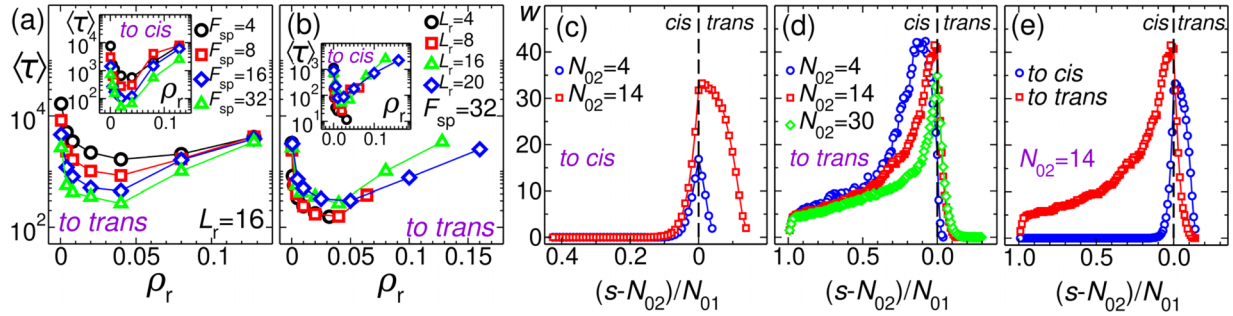
FIG. 3. (a) Mean translocation time $\langle\tau\rangle$ as a function of the rod density ρ_r for fixed rod length $L_r = 16$ and various values of the SP force F_{sp} in the *to-trans* state for the values of the *trans*-side polymer subchain contour length on the boundaries depicted in the Fig. 2(c). Inset shows the same quantity as in the main panel for the *to-cis* state. (b) Same as the panel (a) but for fixed value of the SP force $F_{sp} = 32$ and various values of the rod length L_r. Inset presents the same quantity as the main panel for the *to-cis* state. (c) Waiting time distribution w as a function of normalized and rescaled translocation coordinate $(s - N_{02})/N_{01}$ with $N_{02} = 4$ (blue line - circles) and 14 (red line - squares) for the *to-cis* state. (d) The same quantity as panel (c) but for the *to-trans* state with $N_{02} = 4$ (blue line - circles), 14 (red line - squares), and 30 (green line - diamonds). (e) The same quantity as in panels (c) and (d) for fixed value of $N_{02} = 14$ and for the *to-cis* (blue line - circles) and *to-trans* (red line - squares) states. In panels (c), (d), and (e) the values of the rod length, SP force, and number of rods in the *trans* side are fixed at $L_r = 16$, $F_{sp} = 4$, and $\rho_r = 0.04$ ($N_r = 100$), respectively, and the vertical black dashed line denotes the pore position.

translocation probabilities explained in Fig. 2(a). The pink region above and the gray below the black curve correspond to the *to-trans* and *to-cis* states, respectively. The top and the bottom insets show typical final configurations of the system with fixed values of $L_r = 16$, $F_{sp} = 4$, $N_{02} = N_{02,m} = 14$, and $\rho_r = 0.04$ ($N_r = 100$). As can be seen, the polymer is sucked into the active *trans*-side region if a folded structure is induced in the polymer configuration by the interaction between polymer and ARs (top inset). On the other hand, the polymer leaves the pore towards the *cis* side in the absence of such a folded structure (bottom inset). The configurations of the polymer in the *cis* and in the *trans* sides will be described in detail in Sec. III D.

To investigate the effect of SP force on the border between the *to-cis* and *to-trans* states, Fig. 2(c) shows a diagram in the $N_{02,m} - \rho_r$ plane for fixed value of the rod length $L_r = 16$ and various values of SP force $F_{sp} = 4$ (black line - circles), 8 (red line - squares), 16 (blue line - diamonds), and 32 (green line - triangles). The regions above and below each curve represent the *to-trans* and *to-cis* states, respectively, for the corresponding SP force. Panel (d) in Fig. 2 is the same as panel (c) but for fixed value of SP force $F_{sp} = 32$ and different values of the rod length $L_r = 4$ (black line - circles), 8 (red line - squares), 16 (green line - triangles), and 20 (blue line - diamonds). In the absence of ARs in the *trans* side, for $N_{01} = N_{02} = 100$ the polymer translocates equally either to the *trans* side or retracts back to the *cis* side, i.e., $N_{02} = N_{02,m} = 100$ (not shown here).

By increasing the number of ARs in the *trans* side for the values of the system parameters in the present study, the effective net force on the monomer inside the pore towards the *trans* side increases due to the interactions between the ARs and the *trans*-side polymer subchain (see Appendix B). This increases the probability of successful events [65] leading to smaller values of $N_{02,m}$. On the other hand, for large values of the rod length L_r and increasing the rod density ρ_r, the crowding effect due to the presence of ARs in the vicinity of the nanopore in the *trans* side can block translocation *to-trans*, which leads to larger values of $N_{02,m}$. For small values of the

rod length [cf. Fig. 2(d)], $N_{02,m}$ is a monotonically decreasing function of ρ_r due to negligible crowding.

B. Mean translocation time

The central quantity that reveals the dynamics of the translocation process at the global level is the mean translocation time, which is the time it takes for the whole polymer to enter the *trans* side (translocation time for the *to-trans* state). On the other hand, the time it takes for the polymer to completely retract and enter the *cis* side will be defined as the translocation time for the *to-cis* state.

In the main panel of Fig. 3(a), the mean translocation time $\langle\tau\rangle$ for the *to-trans* state is plotted as a function of the rod density in the *trans* side ρ_r, for fixed $L_r = 16$ and various values of the SP force $F_{sp} = 4$ (black line - circles), 8 (red line - squares), 16 (blue line - diamonds), and 32 (green line - triangles) [cf. Fig. 2(c)]. The inset shows the same quantity as in the main panel but for the *to-cis* state. Panel (b) of Fig. 3 is the same as panel (a) but for fixed values of the SP force $F_{sp} = 32$ and for different values of the rod length $L_r = 4$ (black line - circles), 8 (red line - squares), 16 (green line - triangles), and 20 (blue line - diamonds). Some typical translocation time distributions are shown in Appendix C.

As mentioned before, the top snapshot in the inset of Fig. 2(b) clearly shows that the polymer is sucked into the active environment in the *trans* side if a folded structure is induced on the *trans*-side polymer subchain by the ARs. The main panels in Figs. 3(a) and 3(b), which are for the *to-trans* state, show interesting nonmonotonic behavior of the translocation time. For small densities the effective force first increases and the mean translocation time decreases together with N_{02}. The fastest translocation occurs at around $\rho_r \approx 0.04$, where also $N_{02,m}$ has a minimum, after which the translocation time starts to increase as crowding of the rods becomes relevant. It is interesting to note that the position of the minimum is almost independent of the activity force and the rod length in the range of parameters studied here. In the insets of panels
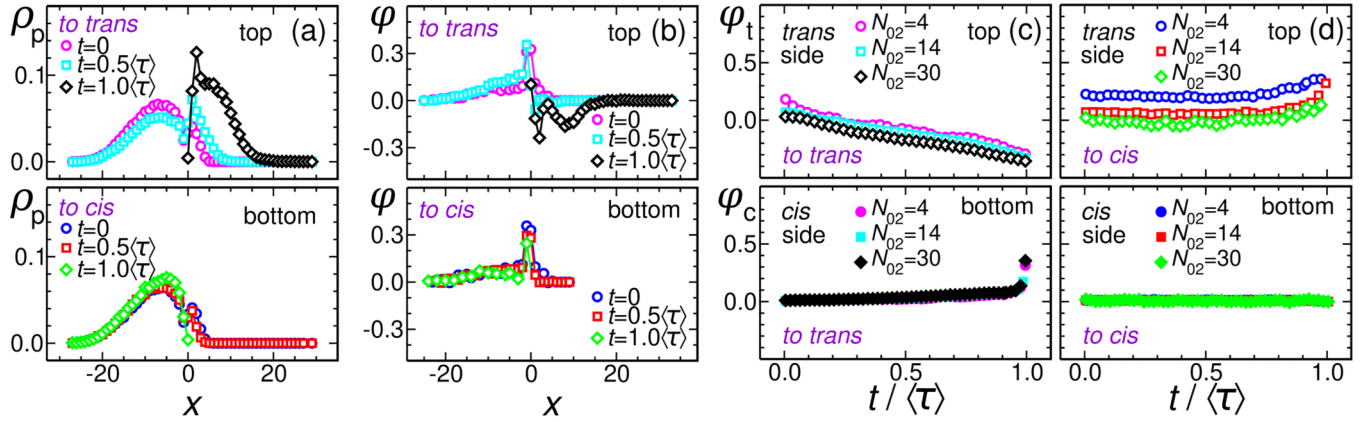
FIG. 4. (a) Top and bottom panels show the monomer number density of the polymer chain for the *to-trans* and *to-cis* states, respectively, as a function of the distance from the nanopore x (pore is at $x = 0$) at times $t = 0$ (top: open pink circles, bottom: open blue circles), $t = 0.5\langle\tau\rangle$ (top: open turquoise squares, bottom: open red squares) and $t = 1.0\langle\tau\rangle$ (top: open black diamonds, bottom: open green diamonds), with fixed values of $L_r = 16$, $\rho_r = 0.04$ ($N_r = 100$), $F_{sp} = 4$, and $N_{02} = N_{02m} = 14$ for all panels. (b) Top: Bond-orientation order parameter $\phi(x)$ for the *to-trans* state as a function of the distance to the pore x at $t = 0$ (open pink circles), $t = 0.5\langle\tau\rangle$ (open turquoise squares), and $t = 1.0\langle\tau\rangle$ (open black diamonds). Bottom: The same as top panel but for the *to-cis* state. (c) Top: Bond-orientation order parameter in the *trans* side ϕ_t as a function of normalized time $t/\langle\tau\rangle$, for the *to-trans* state with initial values of the polymer subchain contour length in the *trans* side $N_{02} = 4$ (open pink circles), 14 (open turquoise squares), and 30 (open black diamonds). Bottom: Order parameter on the *cis* side ϕ_c as a function of normalized time $t/\langle\tau\rangle$, for the *to-trans* state with initial values of the polymer subchain contour length in the *trans* side $N_{02} = 4$ (filled pink circles), 14 (filled turquoise squares), and 30 (filled black diamonds). (d) The same as panel (c) but for the *to-cis* state.

(a) and (b) in Fig. 3 we show data for the *to-cis* state, and the behavior of the translocation time is very similar to that of the *to-trans* state.

C. Waiting time distribution

An important quantity which shows the translocation dynamics at the monomer level is the waiting time (WT) distribution, which is the time that each bead spends at the nanopore during the course of translocation process. In order to present the difference between the *to-cis* and *to-trans* states, in panels (c), (d), and (e) in Fig. 3 the WT distribution w has been plotted as a function of $(s - N_{02})/N_{01}$, where s is the monomer index minus 1, for fixed values of the rod length, SP force, and rod density $L_r = 16$, $F_{sp} = 4$, and $\rho_r = 0.04$ (corresponding to $N_r = 100$), respectively.

Panel (c) in Fig. 3 shows the WT distribution (w) of the *to-cis* state for the initial *tans*-side polymer subchain contour lengths $N_{02} = 4$ (blue line - circles) and 14 (red line - squares). Obviously, increasing N_{02} slows down the dynamics. Panel (d) is the same as (c) but for the *to-trans* state for $N_{02} = 4$ (blue line - circles), 14 (red line - squares), and 30 (green line - diamonds). Here, the waiting time decreases as it becomes more probable to form a larger fold for increasing N_{02}. Finally, panel (e) compares the WT distributions for the *to-cis* (blue line - circles) and *to-trans* (red line - squares) states when the value of the initial *trans*-side polymer subchain contour length lies on the border curve in the phase diagram in Fig. 2(b) with $N_{02} = N_{02,m} = 14$ for $\rho_r = 0.04$.

D. The polymer structure

To further clarify the role of the folds in the *trans* side that assist translocation *to-trans*, we have performed a more detailed analysis of the polymer configurations during

translocation. In the top panel of Fig. 4(a) we plot the monomer number density profile of the polymer chain ρ_p as a function of the distance from the nanopore x at different times $t = 0$ (pink circles), $0.5\langle\tau\rangle$ (turquoise squares), and $1.0\langle\tau\rangle$ (black diamonds) for the *to-trans* state. The *cis* and the *trans* sides are at $x < 0$ and $x > 0$, respectively, and the nanopore at $x = 0$. The bottom panel of (a) shows the same data for the *to-cis* state. The crowding of the monomers close to the pore in the *trans* side indicates that the polymer has folds for the *to-trans* state.

To quantify this, we define the bond-orientation order parameter with respect to the membrane as

$$\phi(x_i) = \left\langle \frac{1}{n_i(t)} \sum_{k=1}^{n_i(t)} [1 - 2(\hat{e}_{i,k} \cdot \hat{u}_y)^2] \right\rangle, \quad (6)$$

where x_i is the horizontal coordinate of a bin (a thin slab parallel to the wall with thickness of unity), $n_i(t)$ is the number of polymer bonds located in the ith bin at time t, $\hat{e}_{i,k}$ is the unit vector of the kth bond in the ith bin, $\hat{u}_y$ is a unit vector parallel to the membrane (y axis), and $\langle \cdots \rangle$ denotes an ensemble average. This quantity measures the average orientation of the bond vectors with respect to the wall. The value of ϕ varies between $[-1, +1]$, and its value is 1, -1, or 0 if the bond orientations are perpendicular, parallel, or randomly distributed with respect to the membrane, respectively.

In the top panel of Fig. 4(b) we plot the order parameter $\phi(x)$ for the *to-trans* state as a function of $x = x_i$, at different moments $t = 0$ (pink circles), $t = 0.5\langle\tau\rangle$ (turquoise squares), and $t = 1.0\langle\tau\rangle$ (black diamonds). With the passage of the time, a spatially oscillating profile forms on the *trans* side, indicating a folded structure. In the bottom panel of (b) for the *to-cis* state the profile remains mostly flat.

Another useful way to quantify the configurations is to divide the order parameter into two spatially averaged
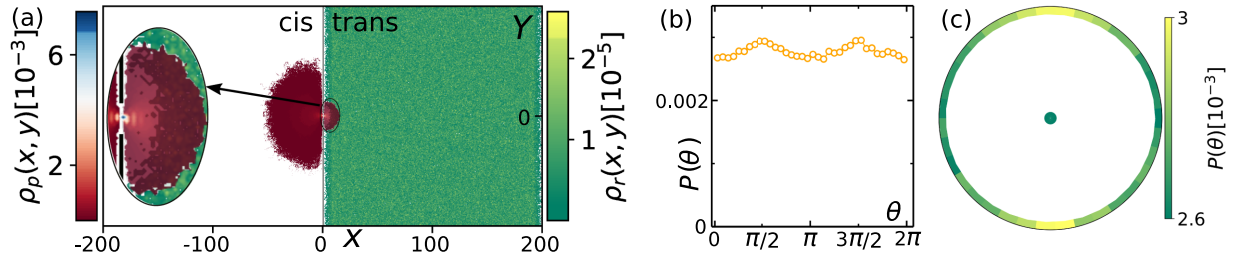
FIG. 5. (a) The probability density profile of monomers $\rho_p(x, y)$ in the *cis*/*trans* sides (left bar) and the rods' center of mass $\rho_r(x, y)$ in the *trans* side (right bar) at $t = 0$ just after the equilibration stage for fixed values of $N_{01} = 100$, $N_{02} = 14$, $L_r = 16$, and $\rho_r = 0.04$ (corresponding to $N_r = 100$). The membrane is set at $x = 0$, and the pore is located at $(x, y) = (0, 0)$. (b) The probability distribution function of the rods' orientation as a function of θ (the angle between the main axis of the rod and the x direction) for the same parameters as of panel (a). The two peaks at $\theta = \pi/2$ and $\theta = 3\pi/2$ are due to excluded volume effects and correspond to rods in the vicinity of the membrane and in the vicinity of the right wall parallel to the membrane located at $x = 200$. (c) The probability distribution function of the rods' orientation in polar coordinates that are distributed on a circle with radius one at $t = 0$ for the same parameters as in panels (a) and (b).

components that evolve in time. They are defined as

$$\phi_t(t) = \left\langle \frac{1}{n_t(t)} \sum_{k=1}^{n_t(t)} [1 - 2(\hat{e}_k \cdot \hat{u}_y)^2] \right\rangle;$$

$$\phi_c(t) = \left\langle \frac{1}{n_c(t)} \sum_{k=1}^{n_c(t)} [1 - 2(\hat{e}_k \cdot \hat{u}_y)^2] \right\rangle, \quad (7)$$

respectively, where $\hat{e}_k$ is the unit bond vector for the kth bond, either in the *trans* side in $\phi_t(t)$ or in the *cis* side in $\phi_c(t)$, and $n_t(t)$ and $n_c(t)$ are the total number of bonds in the *trans* and in the *cis* sides, respectively, at time t.

These *trans*- and *cis*-side components are plotted in Figs. 4(c) and 4(d) for *to-trans* and *to-cis* states, respectively, as a function of the normalized time $t/\langle \tau \rangle$. The negative values of $\phi_t(t)$ as time progresses indicate folds in the *trans* side for the *to-trans* state. At the same time, tension propagates in the *cis* side, as shown in more detail in the SI, making $\phi_c(t)$ positive, because the bonds tend to align perpendicular to the wall. On the other hand, for the *to-cis* state, in the top panel of (d), the *trans*-side polymer subchain retracts to the *cis* side and $\phi_t(t)$ remains positive. Moreover, as can be seen in the bottom panel of (d), for this case the process is very slow and the *cis*-side subchain remains in a state close to equilibrium with $\phi_c(t) \approx 0$.

IV. SUMMARY AND CONCLUSIONS

In the present work we have quantified the role of different physical parameters for active-rod-assisted polymer translocation through a nanopore. In this setup the polymer has a fixed number of N_{01} monomers on the *cis* side of the membrane and a varying number density of active rods (ARs) ρ_r in the *trans* compartment. The interaction between ARs and the polymer in the *trans* side of the subchain with N_{02} initial monomers facilitates successful *to-trans* events even for $N_{02} < N_{01}$, which is not possible for nondriven translocation. We map out a state diagram of successful events in the $N_{02,m} - \rho_r$ plane, revealing competition between facilitation and crowding by the ARs, which results in an optimal value of ρ_r for a minimum value of $N_{02,m}$ and correspondingly, to fastest translocation. We have further done a detailed analysis of the configurations of the translocating polymers which shows that successful

translocation to the *to-trans* state is accompanied by formation of folds in the *trans* side and crowding of the rods near the membrane wall.

It has been suggested that the presence of active particles can induce a high effective temperature in the system [68,69]. We have checked this in the present case and indeed find that the velocity fluctuations are greatly enhanced with increasing activity while their distribution remains Gaussian, as expected for a thermal distribution. As shown in more detail in Appendix D, increasing the activity increases the effective T_{eff} in the *trans* side quadratically as a function of F_{sp}, and for $F_{\text{sp}} = 32$ we find that the effective temperature increases to $T_{\text{eff}}/T = 52.2$. The enhanced success of *to-trans* events with increasing activity can then also be qualitatively understood from a decrease of the (effective) free energy of the chain in the *trans* side, which drives successful translocation events.

These results may shed light on better understanding the polymer translocation process into or out of the living cells, which typically contain various kinds of active particles.

APPENDIX A: EQUILIBRATION OF THE SYSTEM

Before the actual translocation process, the system is carefully equilibrated. During the equilibration stage the self-propelling (SP) force is switched off, i.e., $F_{\text{sp}} = 0$. The total polymer contour length $N_0 = N_{01} + N_{02} + 1$, where $N_{01} = 100$ and N_{02} are the initial length of the subchains in the *cis* and *trans* sides, respectively, and 1 refers to a monomer which is being fixed at the pore during the equilibration stage. The initial configuration of the system is composed of a straightened polymer perpendicular to the membrane with the above lengths in the *cis* and the *trans* sides, and N_r rods which are only in the *trans* side uniformly distributed. Then, after the simulation is run for $\tau_{\text{eq}} = 5 \times 10^5 \tau_0$, where τ_0 is the
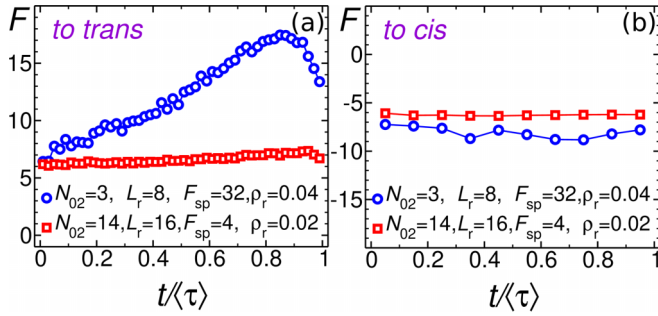
FIG. 6. (a) The effective force F as a function of the normalized time $t/\langle\tau\rangle$ for the *to-trans* state, for two sets of parameters: (1) $N_{02} = 3$, $L_r = 8$, $F_{sp} = 32$, and $\rho_r = 0.04$ (blue line - circles), and (2) $N_{02} = 14$, $L_r = 16$, $F_{sp} = 4$, and $\rho_r = 0.02$ (red line - squares). (b) The same as panel (a) but for the *to-cis* state.

Lennard-Jones unit of time, both polymer and rods become equilibrated as shown in Fig. 5. Here the initial value of the *trans*-side subchain is $N_{02} = 14$. Panel (a) shows the probability density profile of the polymer beads in the *cis/trans* sides (left bar) and the probability density profile of the rods' center of mass in the *trans* side of the membrane (right bar). Panel (b) is the probability distribution function of the rods' orientations. The two peaks at $\theta = \pi/2$ and $\theta = 3\pi/2$ correspond to the rods in the vicinity of the membrane and the right wall parallel to the membrane at $x = 200$ due to the excluded volume effects. θ is the angle between each rod's main axial (parallel to the rod) unit vector and the x axis. Panel (c) shows the probability distribution function of the rods' orientations that are distributed on a circle with radius unity. As all these panels show, the system is well equilibrated.

APPENDIX B: EFFECTIVE FORCE AT THE NANOPORE

In Fig. 6(a) the effective force F acting on the monomer inside the nanopore has been plotted as a function of the normalized time $t/\langle\tau\rangle$ for the *to-trans* state, for two sets of parameters: (1) $N_{02} = 3$, $L_r = 8$, $F_{sp} = 32$, and $\rho_r = 0.04$ (blue line - circles) that have been chosen from a data point on the red line with squares in panel (d) of Fig. 2, and (2) $N_{02} = 14$,

$L_r = 16$, $F_{sp} = 4$, and $\rho_r = 0.02$ (red line with squares) that have been chosen from a data point on the black line with squares in panel (c) of Fig. 2. The effective force F is the sum of the interactions of the ARs with the monomer inside the nanopore and the tension due to the *trans*-side subchain experienced by the monomer inside the nanopore. As can be seen, for both cases the effective force first increases linearly and then decreases, which is a characteristic signature of tension propagation along the backbone of the subchain in the *cis* side. Panel (b) in Fig. 6 is the same as panel (a) but for the *to-cis* state. Here, the effective force F is the sum of the AR interactions with the monomer inside the nanopore and the tension due to the *cis*-side subchain acting on the monomer inside the nanopore.

APPENDIX C: DISTRIBUTION OF TRANSLOCATION TIMES

Figure 7(a) shows the probability distribution function of the translocation time $P(\tau)$ for the *to-cis* state with fixed values of $L_r = 16$ and $F_{sp} = 4$ and various values of the density of rods in the *trans* side $\rho_r = 0.004$ (violet bars), 0.008 (red bars), 0.02 (green bars), 0.04 (pink bars), and 0.08 (turquoise bars), corresponding to the number of rods $N_r = 10, 20, 50, 100$, and 200, respectively. These parameters have been chosen from the boundary line in Fig. 2(c) (black line with open circles). Panel (b) in Fig. 7 is the same as Fig. 7(a) but for the *to-trans* state. Panels (c) and (d) are the same as (a) and (b), respectively, but for stronger SP force $F_{sp} = 32$. The parameters of the system in panels (c) and (d) of Fig. 7 have been chosen from the boundary line in Fig. 2(c) (green line with triangles).

APPENDIX D: EFFECTIVE TEMPERATURE INDUCED BY ROD ACTIVITY

To find the effective temperature of the system T_{eff} as a function of the SP force we have performed additional Langevin dynamics simulations with the active rods only in the *trans* side. The parameters of the system are as follows: length of rods is fixed at $L_r = 16$ and the number of rods is $N_r = 100$ corresponding to density $\rho_r = 0.04$. As seen
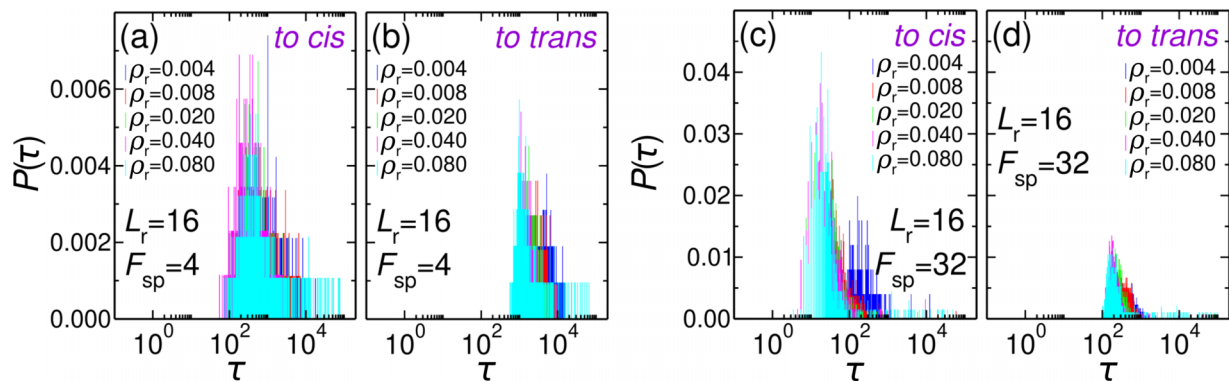

FIG. 7. (a) Probability distribution function of the translocation time $P(\tau)$ as a function of τ for the *to-cis* state with fixed values of $L_r = 16$ and $F_{sp} = 4$ for various values of $\rho_r = 0.004$ (violet bars), 0.008 (red bars), 0.02 (green bars), 0.04 (pink bars), and 0.08 (turquoise bars). (b) The same as (a) but for the *to-trans* state. Panels (c) and (d) are the same as panels (a) and (b), respectively, but for a stronger SP force $F_{sp} = 32$.
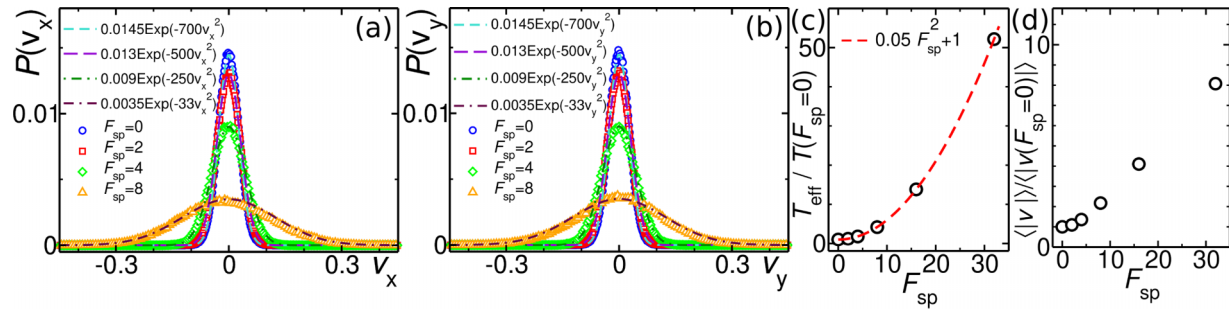
FIG. 8. (a) The probability distribution function $P(v_x)$ of the x component of the velocity v_x for the self-propelling (SP) force $F_{sp} = 0$ (blue circles), 2 (red squares), 4 (green diamonds), and 8 (orange triangles). The lines represent Gaussian fitting functions to each set of data. (b) The same as panel (a) but for the y component of the velocity. (c) The normalized effective temperature $T_{eff}/T(F_{sp} = 0)$ as a function of SP force F_{sp}. The red dashed line is a quadratic fitting function as indicated inside the panel. The temperature of the passive system is $T(F_{sp} = 0) = 1.2$. The effective temperature of the active system T_{eff} has been obtained by considering the equipartition theorem $\langle \frac{1}{2}mv^2 \rangle = \frac{1}{2}k_B T_{eff} + \frac{1}{2}k_B T_{eff} = k_B T_{eff}$ for two degrees of freedom for each particle in two dimensions. (d) The average value of the normalized speed $\langle |v| \rangle / \langle |v(F_{sp} = 0)| \rangle$ as a function of the SP force F_{sp}.

in Figs. 8(a) and 8(b), the probability distribution functions (PDFs) of the x and the y components of the velocity are Gaussian. In panel (c) the normalized effective temperature $T_{eff}/T(F_{sp} = 0)$ has been plotted as a function of the SP force F_{sp} (black circles). The red dashed line is a quadratic fitting function $1 + 0.05F_{sp}^2$. It can be seen that the effective temperature quadratically increases as the value of the SP force

increases. The temperature of the passive system is $T(F_{sp} = 0) = 1.2$. The effective temperature of the active system T_{eff} has been obtained by considering the equipartition theorem $\langle \frac{1}{2}mv^2 \rangle = \frac{1}{2}k_B T_{eff} + \frac{1}{2}k_B T_{eff} = k_B T_{eff}$ for two degrees of freedom for each particle in two dimensions. Panel (d) presents the average value of the normalized speed $\langle |v| \rangle / \langle |v(F_{sp} = 0)| \rangle$ as a function of the SP force F_{sp}.

[1] S. M. Bezrukov, I. Vodyanoy, and A. V. Parsegian, Counting polymers moving through a single ion channel, Nature (London) **370**, 279 (1994).

[2] J. J. Kasianowicz, E. Brandin, D. Branton, and D. W. Deamer, Characterization of individual polynucleotide molecules using a membrane channel, Proc. Natl. Acad. Sci. USA **93**, 13770 (1996).

[3] W. Sung and P. J. Park, Polymer Translocation through a Pore in a Membrane, Phys. Rev. Lett. **77**, 783 (1996).

[4] A. Meller, L. Nivon and D. Branton, Voltage-Driven DNA Translocations through a Nanopore, Phys. Rev. Lett. **86**, 3435 (2001).

[5] D. E. Smith, S. J. Tans, S. B. Smith, S. Grimes, D. L. Anderson, and C. Bustamante, The bacteriophage straight phi29 portal motor can package DNA against a large internal force, Nature (London) **413**, 748 (2001).

[6] A. J. Storm, J. H. Chen, X. S. Ling, H. W. Zandbergen and C. Dekker, Fabrication of solid-state nanopores with single-nanometre precision, Nat. Mater. **2**, 537 (2003).

[7] A. F. Sauer-Budge, J. A. Nyamwanda, D. K. Lubensky and D. Branton, Unzipping Kinetics of Double-Stranded DNA in a Nanopore, Phys. Rev. Lett. **90**, 238101 (2003).

[8] A. J. Storm, C. Storm, J. Chen, H. Zandbergen, J.-F. Joanny and C. Dekker, Fast DNA translocation through a solid-state nanopore, Nano Lett. **5**, 1193 (2005).

[9] U. F. Keyser, B. N. Koeleman, S. van Dorp, D. Krapf, R. M. M. Smeets, S. G. Lemay, N. H. Dekker, and C. Dekker, Direct force measurements on DNA in a solid-state nanopore, Nat. Phys. **2**, 473 (2006).

[10] S. Van Dorp, U. F. Keyser, N. H. Dekker, C. Dekker, and S. G. Lemay, Origin of the electrophoretic force on DNA in solid-state nanopores, Nat. Phys. **5**, 347 (2009).

[11] R. D. Bulushev, S. Marion and A. Radenovic, Relevance of the drag force during controlled translocation of a DNA–protein complex through a glass nanocapillary, Nano Lett. **15**, 7118 (2015).

[12] J.-W. Yeh, A. Taloni, Y.-L. Chen and C.-F. Chou, Entropy-driven single molecule tug-of-war of DNA at micro-nanofluidic interfaces, Nano Lett. **12**, 1597 (2012).

[13] M. Muthukumar, *Polymer Translocation* (Taylor and Francis, London, 2011).

[14] V. V. Palyulin, T. Ala-Nissila, and R. Metzler, Polymer translocation: The first two decades and the recent diversification, Soft Matter **10**, 9016 (2014).

[15] A. Milchev, Single-polymer dynamics under constraints: Scaling theory and computer experiment, J. Phys.: Condens. Matter **23**, 103101 (2011).

[16] J. Sarabadani and T. Ala-Nissila, Theory of pore-driven and end-pulled polymer translocation dynamics through a nanopore: An overview, J. Phys.: Condens. Matter **30**, 274002 (2018).

[17] M. Muthukumar, Polymer translocation through a hole, J. Chem. Phys. **111**, 10371 (1999).

[18] Y. Kantor and M. Kardar, Anomalous dynamics of forced translocation, Phys. Rev. E **69**, 021806 (2004).

[19] A. Y. Grosberg, S. Nechaev, M. Tamm, and O. Vasilyev, How Long Does It Take to Pull an Ideal Polymer into a Small Hole? Phys. Rev. Lett. **96**, 228105 (2006).

[20] G. Sigalov, J. Comer, G. Timp, and A. Aksimentiev, Detection of DNA sequences using an alternating electric field in a nanopore capacitor, Nano Lett. **8**, 56 (2008).

[21] P. Rowghanian and A. Y. Grosberg, Force-driven polymer translocation through a nanopore: An old problem revisited, J. Phys. Chem. B **115**, 14127 (2011).

[22] T. Sakaue, Nonequilibrium dynamics of polymer translocation and straightening, Phys. Rev. E **76**, 021803 (2007).

[23] T. Sakaue, Nonequilibrium dynamics of polymer translocation and straightening, Phys. Rev. E **81**, 041808 (2010).

[24] T. Saito and T. Sakaue, Process time distribution of driven polymer transport, Phys. Rev. E **85**, 061803 (2012).

[25] I. Huopaniemi, K. Luo, T. Ala-Nissila, and S.-C. Ying, Polymer translocation through a nanopore under a pulling force, Phys. Rev. E **75**, 061912 (2007).

[26] T. Ikonen, A. Bhattacharya, T. Ala-Nissila, and W. Sung, Unifying model of driven polymer translocation, Phys. Rev. E **85**, 051803 (2012).

[27] T. Ikonen, A. Bhattacharya, T. Ala-Nissila, and W. Sung, Influence of non-universal effects on dynamical scaling in driven polymer translocation, J. Chem. Phys. **137**, 085101 (2012).

[28] J. Sarabadani, T. Ikonen, and T. Ala-Nissila, Iso-flux tension propagation theory of driven polymer translocation: The role of initial configurations, J. Chem. Phys. **141**, 214907 (2014).

[29] J. Sarabadani, T. Ikonen, and T. Ala-Nissila, Theory of polymer translocation through a flickering nanopore under an alternating driving force, J. Chem. Phys. **143**, 074905 (2015).

[30] J. Sarabadani, B. Ghosh, S. Chaudhury, and T. Ala-Nissila, Dynamics of end-pulled polymer translocation through a nanopore, Europhys. Lett. **120**, 38004 (2017).

[31] T. Menais, S. Mossa, and A. Buhot, Polymer translocation through nano-pores in vibrating thin membranes, Sci. Rep. **6**, 38558 (2017).

[32] J. Sarabadani, T. Ikonen, H. Mökkönen, T. Ala-Nissila, S. Carson, and M. Wanunu, Driven translocation of a semi-flexible polymer through a nanopore, Sci. Rep. **7**, 7423 (2017).

[33] H. W. de Haan and G. W. Slater, Using an incremental mean first passage approach to explore the viscosity dependent dynamics of the unbiased translocation of a polymer through a nanopore, J. Chem. Phys. **136**, 204902 (2012).

[34] H. W. de Haan and G. W. Slater, Mapping the variation of the translocation scaling exponent with nanopore width, Phys. Rev. E **81**, 051802 (2010).

[35] M. G. Gauthier and G. W. Slater, Nondriven polymer translocation through a nanopore: Computational evidence that the escape and relaxation processes are coupled, Phys. Rev. E **79**, 021802 (2009).

[36] N. Nikoofard, H. Khalilian, and H. Fazli, Directed translocation of a flexible polymer through a cone-shaped nano-channel, J. Chem. Phys. **139**, 074901 (2013).

[37] S. Buyukdagli, J. Sarabadani, and T. Ala-Nissila, Dielectric trapping of biopolymers translocating through insulating membranes, Polymers **10**, 1242 (2018).

[38] S. Buyukdagli, J. Sarabadani, and T. Ala-Nissila, Theoretical modeling of polymer translocation: From the electrohydrodynamics of short polymers to the fluctuating long polymers, Polymers **11**, 118 (2019).

[39] J. Sarabadani, S. Buyukdagli, and T. Ala-Nissila, Pulling a DNA molecule through a nanopore embedded in an anionic membrane: Tension propagation coupled to electrostatics, J. Phys.: Condens. Matter **32**, 385101 (2020).

[40] A. Bhattacharya and S. Seth, Tug of war in a double-nanopore system, Phys. Rev. E **101**, 052407 (2020).

[41] B. Ghosh, J. Sarabadani, S. Chaudhury, and T. Ala-Nissila, Pulling a folded polymer through a nanopore, J. Phys.: Condens. Matter **33**, 015101 (2021).

[42] J. A. Cohen, A. Chaudhuri, and R. Golestanian, Active Polymer Translocation through Flickering Pores, Phys. Rev. Lett. **107**, 238102 (2011).

[43] T. Menais, Polymer translocation under a pulling force: Scaling arguments and threshold forces, Phys. Rev. E **97**, 022501 (2018).

[44] R. Adhikari and A. Bhattacharya, Translocation of a semiflexible polymer through a nanopore in the presence of attractive binding particles, Phys. Rev. E **92**, 032711 (2015).

[45] Z. Fazli and A. Naji, Rectification of polymer translocation through nanopores by nonchiral and chiral active particles, Phys. Rev. E **107**, 024602 (2023).

[46] J. Sarabadani, R. Metzler, and T. Ala-Nissila, Driven polymer translocation into a channel: Isoflux tension propagation theory and Langevin dynamics simulations, Phys. Rev. Res. **4**, 033003 (2022).

[47] S. Nakielny and G. Dreyfuss, Transport of proteins and RNAs in and out of the nucleus, Cell **99**, 677 (1999).

[48] L. Messager, J. R. Burns, J. Kim, D. Cecchin, J. Hindley, A. L. B. Pyne, J. Gaitzsch, G. Battaglia, and S. Howorka, Biomimetic hybrid nanocontainers with selective permeability, Angew. Chem. Int. Ed. **55**, 11106 (2016).

[49] D. Branton, D. W. Deamer, A. Marziali, H. Bayley, S. A. Benner, T. Butler, M. Di Ventra, S. Garaj, A. Hibbs, X. Huang *et al.*, The potential and challenges of nanopore sequencing, Nat. Biotechnol. **26**, 1146 (2008).

[50] D. Deamer, M. Akeson, and D. Branton, Three decades of nanopore sequencing, Nat. Biotechnol. **34**, 518 (2016).

[51] H. Ochman, J. G. Lawrence, and E. A. Groisman, Lateral gene transfer and the nature of bacterial innovation, Nature (London) **405**, 299 (2000).

[52] B. Alberts, A. Johnson, J. Lewis, M. Raff, K. Roberts, and P. Walter, *Molecular Biology of the Cell* (Garland Science, New York, 2002).

[53] A. Gopinathan and Y. W. Kim, Polymer Translocation in Crowded Environments, Phys. Rev. Lett. **99**, 228106 (2007).

[54] Y. Chen and K. Luo, Dynamics of polymer translocation through a nanopore induced by different sizes of crowding agents, J. Chem. Phys. **138**, 204903 (2013).

[55] W. Yu and K. Luo, Polymer translocation through a nanopore driven by binding particles: Influence of chain rigidity, Phys. Rev. E **90**, 042708 (2014).

[56] F. Samadi Taheri, H. Fazli, M. Doi, and M. Habibi, Granular chain escape from a pore in a wall in the presence of particles on one side: A comparison to polymer translocation, Soft Matter **14**, 5420 (2018).

[57] R. H. Abdolvahab, M. R. Ejtehadi, and R. Metzler, Sequence dependence of the binding energy in chaperone-driven polymer translocation through a nanopore, Phys. Rev. E **83**, 011902 (2011).

[58] S. Emamyari and H. Fazli, Polymer translocation through a nanopore in the presence of chaperones: A three dimensional MD simulation study, Comput. Condens. Matter **13**, 96 (2017).

[59] X. Xu and Y. Zhang, Mean velocity and effective diffusion constant for translocation of biopolymer chains across membrane, J. Stat. Mech. **2020**, 023501 (2020).

[60] F. Ritort, Single-molecule experiments in biological physics: Methods and applications, J. Phys.: Condens. Matter **18**, R531 (2006).

[61] A. Sischka, A. Spiering, M. Khaksar, M. Laxa, J. Konig, K.-J. Dietz, and D. Anselmetti, Dynamic translocation of ligand-complexed DNA through solid-state nanopores with optical tweezers, J. Phys.: Condens. Matter **22**, 454121 (2010).

[62] R. D. Bulushev, L. J. Steinbock, S. Khlybov, J. F. Steinbock, U. F. Keyser, and A. Radenovic, Measurement of the position-dependent electrophoretic force on DNA in a glass nanocapillary, Nano Lett. **14**, 6606 (2014).

[63] M. Pu, H. Jiang, and Z. Hou, Polymer translocation through nanopore into active bath, J. Chem. Phys. **145**, 174902 (2016).

[64] F. Tan, Y. Chen, and N. Zhao, Effects of active crowder size and activity–crowding coupling on polymer translocation, Soft Matter **17**, 1940 (2021).

[65] H. Khalilian, J. Sarabadani, and T. Ala-Nissila, Polymer translo-cation through a nanopore assisted by an environment of active rods, Phys. Rev. Res. **3**, 013080 (2021).

[66] G. S. Grest and K. Kremer, Molecular dynamics simulation for polymers in the presence of a heat bath, Phys. Rev. A **33**, 3628 (1986).

[67] S. Plimpton, Fast parallel algorithms for short-range molecular dynamics, J. Comput. Phys. **117**, 1 (1995); http://lammps.sandia.gov.

[68] J. Shin, A. G. Cherstvy, W. K. Kim, and R. Metzler, Facilitation of polymer looping and giant polymer diffusivity in crowded solutions of active particles, New J. Phys. **17**, 113008 (2015).

[69] X. Cao, B. Zhang, and N. Zhao, Effective temperature scaled dynamics of a flexible polymer in an active bath, Mol. Phys. **118**, e1730992 (2020).